Magnetic ordering of $R_3Cu_4Sn_4$ (R = Tb, Dy, Ho and Er)

2003 J. Phys.: Condens. Matter 15 5279

(http://iopscience.iop.org/0953-8984/15/30/310)

INSTITUTE OF PHYSICS PUBLISHING JOURNAL OF PHYSICS: CONDENSED MATTER

J. Phys.: Condens. Matter **15** (2003) 5279–5296 PII: S0953-8984(03)60506-0

Magnetic ordering of $R_3Cu_4Sn_4$ (R = Tb, Dy, Ho and Er)

E Wawrzyńska[1], J Hernandez-Velasco[2], B Penc[1], W Sikora[3], A Szytuła[1] and A Zygmunt[4]

[1] M Smoluchowski Institute of Physics, Jagiellonian University, Reymonta 4, 30-059 Kraków, Poland
[2] BENSC, Hahn-Meitner Institut, Glienicker Straße 100, D-14109 Berlin-Wannsee, Germany
[3] Faculty of Physics and Nuclear Techniques, University of Mining and Metallurgy, Reymonta 19, 30-059 Kraków, Poland
[4] W Trzebiatowski Institute of Low Temperature and Structure Research, Polish Academy of Sciences, Dorodna 2, 50-950 Wrocław, Poland

E-mail: wawrzyn@castor.if.uj.edu.pl

Received 7 April 2003, in final form 14 May 2003
Published 18 July 2003
Online at stacks.iop.org/JPhysCM/15/5279

Abstract

Neutron diffraction studies of polycrystalline $R_3Cu_4Sn_4$ (R = Tb, Dy, Ho, Er) intermetallic compounds with the orthorhombic $Gd_3Cu_4Ge_4$-type crystal structure indicate the existence of different magnetic structures. Rare earth atoms occupy two non-equivalent 2d and 4e sublattices. The rare earth magnetic moments order at low temperatures. For R = Tb and Dy the magnetic structures below the Néel temperature are described by the propagation vectors $\boldsymbol{k} = (0, 0, \frac{1}{2} + \delta)$. In these compounds both rare earth sublattices order. For R = Ho the magnetic structure is more complicated. There are two vectors; one of them is $\boldsymbol{k} = (0, \frac{1}{2}, 0)$ whereas the second one changes with temperature. For the Er compound there is the propagation vector $\boldsymbol{k} = (\frac{1}{2}, \frac{1}{2}, 0)$ which describes the magnetic ordering in the 2d sublattice and at low temperatures is accompanied by the propagation vector $\boldsymbol{k} = (0, 0, \delta)$ describing the ordering in the 4e sublattice.

1. Introduction

This investigation is a part of a broader study which is expected to systematize the magnetic properties (including the magnetic structures) of the $R_mT_nX_p$ rare earth intermetallic compounds, where R is a rare earth atom, T is a d-electron atom and X is a p-electron atom. According to the x-ray data the $R_3Cu_4Sn_4$ (R = Tb, Dy, Ho, Er) compounds investigated in this work crystallize in the orthorhombic $Gd_3Cu_4Ge_4$-type crystal structure (*Immm* space group). In these compounds the rare earth atoms occupy two different crystallographic sublattices [1]. A similar situation is observed in the $RTGe_2$ (R = heavy rare earth atom,

T = Ir, Pt) compounds, which crystallize in the orthorhombic crystal structure (*Immm* space group); the rare earth atoms occupy two non-equivalent sublattices [2]. Neutron diffraction data indicate that the rare earth magnetic moments in different sublattices order at different temperatures and form different magnetic orders [3–5]. $R_3Cu_4Sn_4$ (R = Tb, Dy, Ho, Er) compounds are a new class of materials in which it is possible to investigate the similarity of properties. Temperature dependences of magnetic susceptibility in the temperature range 78–293 K for the $R_3Cu_4Sn_4$ (R = Gd–Tm) compounds indicate that they obey the Curie–Weiss law with negative values of paramagnetic Curie temperature for R = Gd–Ho and a positive one for R = Er and Tm. The effective magnetic moments correspond to the free R^{3+} ion values [1]. The new magnetic and specific heat data show that these compounds are antiferromagnets with Néel temperatures equal to 10.4 K (R = Ce) [6, 7], 11.2 K (Pr), 1.8 K (Nd), 9 K (Sm) [8], 13 K (Gd) [6] and 5.8 K (Er) [9]. Below T_N additional phase transitions in the ordered states are detected.

Previously we have also investigated the $R_3Cu_4Ge_4$ (R = Tb, Dy, Ho, Er) compounds [10] and so we have managed to determine their crystal and magnetic structures as functions of temperature. This work may thus be considered as a continuation of previous work. This time we also report the results of x-ray, neutron diffraction and magnetic investigations of structural and magnetic properties of the $R_3Cu_4Sn_4$ compounds, where R = Tb, Dy, Ho and Er.

2. Experimental procedure

Polycrystalline samples of the $R_3Cu_4Sn_4$ (R = Tb, Dy, Ho, Er) compounds, each with a total weight of about 7 g, were synthesized by arc melting of stoichiometric amounts of high-purity elements (3 N purity for R elements and 4 N for Cu and Sn) in a Ti/Zr gettered argon atmosphere. The reaction products were annealed at 800 °C for a week.

In order to check their purity, the samples were examined by x-ray powder diffraction (Cu Kα radiation). The peaks in the x-ray patterns were indexed in the orthorhombic $Gd_3Cu_4Ge_4$-type structure.

Neutron diffractograms were obtained on the E6 instrument at the BERII reactor at the Hahn-Meitner Institut, Berlin. The incident neutron wavelengths were 2.441 Å (for $Tb_3Cu_4Sn_4$) and 2.448 Å (for the remaining compounds). Diffraction patterns were recorded at different temperatures between 1.5 and 20 K. The Rietveld-type program FULLPROF [11] was adopted for processing the neutron diffraction data.

Magnetic data were collected using a SQUID magnetometer in the temperature range 1.5–30 K and in external magnetic fields up to 100 Oe.

3. Symmetry analysis

Models used for refinement of magnetic structures are usually presented as sets of Fourier coefficients describing the magnetic moment components on particular ions. The use of symmetry is restricted to imposing extra constraints for magnetic moments localized on symmetry-equivalent atoms. The method used here is based on the theory of representations of space groups and was first proposed by Bertaut [12] and Izyumov [13]. It gives the possibility of considering all the possible models for magnetic structures consistent with a given crystal structure with symmetry space group G. According to this method the magnetic structure given by $\boldsymbol{S}$ can be expressed in the coordinate system formed by the basis vectors $\Psi_{\lambda}^{k_l,\nu}$ of the irreducible representations of the group G. Such a coordinate system is the best one matching the symmetry of the problem and it provides the simplest form for the magnetic structure

description because it requires the lowest number of independent parameters. $\boldsymbol{S}$ is described as a linear combination of basis vectors (magnetic modes) and is given by

$$\boldsymbol{S} = \sum_{l,\nu,\lambda} c_{\lambda}^{k_l,\nu} \Psi^l \tag{1}$$

where l is the number of $\boldsymbol{k}$ vectors determined by experiment, ν is the number of irreducible representations and λ is the dimension of the νth irreducible representation given by the symmetry of the crystal structure. The symmetry group $G(\boldsymbol{k})$ of the $\boldsymbol{k}$ vectors is a subgroup of the space group G. From this fact it follows that the set of equivalent positions in the group G, the so-called orbit in G, may split into independent sets of equivalent positions in $G(\boldsymbol{k})$. Thus, one orbit in the group G can lead to two or more orbits in the $G(\boldsymbol{k})$ subgroup. The possible relations between the magnetic moments inside a given orbit are limited by symmetry and a single set of parameters describes the magnetic structure of all atoms belonging to the same orbit. Symmetry allows independent magnetic orderings in different orbits. For orbits belonging to different representations, the magnetic moments, phases, etc differ and the magnetic moments localized at atoms belonging to one orbit may order at temperature T_1 while the moments belonging to another orbit may order at T_2. The relations between the different orbits depend on the minimum of energy of the full structure, not on symmetry.

The form of the basis vectors and information about which of the representations take part in the phase transition under consideration are directly given by the theory of groups and representations. In this work we use the computer program MODY [14], which is based on the theory of groups and representations, to calculate this information. It is important to note that the basis vectors have the same translational properties as Bloch functions. Therefore, the basis vectors may be defined *on positions of a given orbit* in the elementary cell of the crystal as well as in the elementary cell translated by a lattice vector $\boldsymbol{t}$, which just corresponds to a multiplication by $e^{i\boldsymbol{k}_1\boldsymbol{t}}$. The different sets of $c_{\lambda}^{k_l,\nu}$ parameters, where $c_{\lambda}^{k_l,\nu}$ may be complex, correspond to different models of the magnetic structure and may be used as good order parameters in the Landau–Ginzburg theory of phase transitions. However, not all of the possible $c_{\lambda}^{k_l,\nu}$ are allowed, because the parameters should be selected in such a way that the resulting magnetic moments related to all atoms have real values. This condition influences the set of equations which the $c_{\lambda}^{k_l,\nu}$ have to satisfy, and as a result the number of independent free parameters is reduced and strictly determined. Because of the Bloch-like form of the basis vectors and the necessity of getting real values for $\boldsymbol{S}$, only one of the $\boldsymbol{k}$ vectors in the set of symmetry related $\boldsymbol{k}$ vectors (the so-called star-of-$\boldsymbol{k}$) has to be included in the linear combination for $\boldsymbol{S}$ (see equation (1)) if the magnetic cell is the same as the crystallographic unit cell or doubled in any direction ($k_i = 0$ or $\frac{1}{2}$). For any other commensurate or incommensurate magnetic structure both the $\boldsymbol{k}$ and $-\boldsymbol{k}$ vectors in the star-of-$\boldsymbol{k}$ must be included in the linear combination describing $\boldsymbol{S}$. The essential fact is that magnetic phase transitions usually take place according to one irreducible representation with a not too large dimension.

4. Results

4.1. Crystal structure

The x-ray patterns recorded at 300 K, as well as the neutron diffraction patterns recorded at 20, 20, 15 and 10 K for $Tb_3Cu_4Sn_4$, $Dy_3Cu_4Sn_4$, $Ho_3Cu_4Sn_4$ and $Er_3Cu_4Sn_4$ respectively, confirmed that these compounds crystallize in the orthorhombic structure of $Gd_3Cu_4Ge_4$-type, described by the $Immm$ space group. In this structure the rare earth atoms occupy two sites, 2d ($\frac{1}{2}$, 0, $\frac{1}{2}$) and 4e (x, 0, 0); the Cu atoms are situated at the 8n (x, y, 0) positions and the Sn atoms are at the 4f (x, $\frac{1}{2}$, 0) and 4h (0, y, $\frac{1}{2}$) positions in the crystal unit cell. The determined

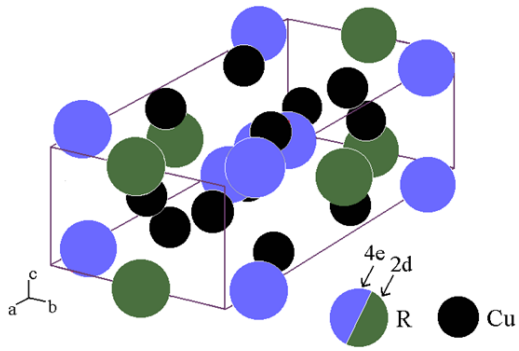

Figure 1. Crystal structure of the $R_3Cu_4Sn_4$ compounds (only R and Cu atoms are presented). (This figure is in colour only in the electronic version)

Table 1. The refined structural parameters of the $R_3Cu_4Sn_4$ (R = Tb, Dy, Ho, Er) compounds (space group *Immm* (No 71)) obtained from the x-ray diffraction patterns at 300 K (labelled by X) and from neutron diffraction data collected at lower temperatures (labelled by N). Standard deviations are given in brackets.

Compound	$Tb_3Cu_4Sn_4$		$Dy_3Cu_4Sn_4$		$Ho_3Cu_4Sn_4$		$Er_3Cu_4Sn_4$	
method	X	N	X	N	X	N	X	N
T (K)	300	20	300	20	300	15	300	10
a (Å)	14.6655(9)	14.623(6)	14.612(1)	14.78(1)	14.5744(8)	14.74(1)	14.5327(8)	14.725(9)
b (Å)	6.9183(4)	6.903(3)	6.9110(5)	6.984(5)	6.9052(3)	6.982(5)	6.8978(3)	6.994(4)
c (Å)	4.4470(3)	4.436(2)	4.4312(3)	4.481(3)	4.4187(2)	4.465(3)	4.4050(2)	4.460(3)
V (Å^3)	451.19(5)	447.7(3)	447.48(6)	462.7(6)	444.70(4)	459.4(5)	441.57(4)	459.3(5)
x_R	0.1317(8)	0.135(1)	0.1279(8)	0.135(1)	0.1338(5)	0.140(2)	0.1285(5)	0.142(2)
x_{Cu}	0.330(1)	0.3314(8)	0.327(1)	0.333(2)	0.3275(7)	0.337(1)	0.3284(7)	0.337(1)
y_{Cu}	0.187(2)	0.182(2)	0.184(2)	0.182(4)	0.183(1)	0.181(2)	0.180(2)	0.180(2)
x_{Sn}	0.2157(8)	0.216(2)	0.2109(8)	0.203(3)	0.2167(5)	0.206(2)	0.2129(5)	0.208(2)
y_{Sn}	0.201(2)	0.208(2)	0.206(2)	0.225(8)	0.203(1)	0.199(3)	0.202(1)	0.205(3)
R_{wp} (%)	24.66[a]	8.92	25.28[a]	10.4	19.59[a]	7.27	19.31[a]	9.59
R_{exp} (%)	15.31[a]	4.65	14.82[a]	5.67	10.30[a]	4.90	9.78[a]	5.28

[a] Large values of the quality-of-fit parameters for the x-ray diffraction patterns are caused by the texture, which came into being during sample preparation.

values of the lattice parameters a, b and c as well as the positional parameters corresponding to the minimum of the reliability factor are listed in table 1. The crystal structure of these compounds is shown in figure 1.

4.2. Magnetic structure

Temperature dependences of magnetization of the $R_3Cu_4Sn_4$ (R = Tb, Dy, Ho, Er) compounds are shown in figure 2. In the cases of $Tb_3Cu_4Sn_4$ and $Dy_3Cu_4Sn_4$ maxima at about 17.5 and 14 K are observed. In the temperature dependence of the magnetization of $Ho_3Cu_4Sn_4$ a jump in the temperature range 1.5–3.5 K and then a broad maximum between 3.5 and 8 K are visible. For $Er_3Cu_4Sn_4$ two maxima at 2.5 and 6 K are detected. The determined values of the magnetic transition temperatures are summarized in table 2. Neutron diffraction patterns recorded at low temperatures reveal the presence of additional peaks of magnetic origin.

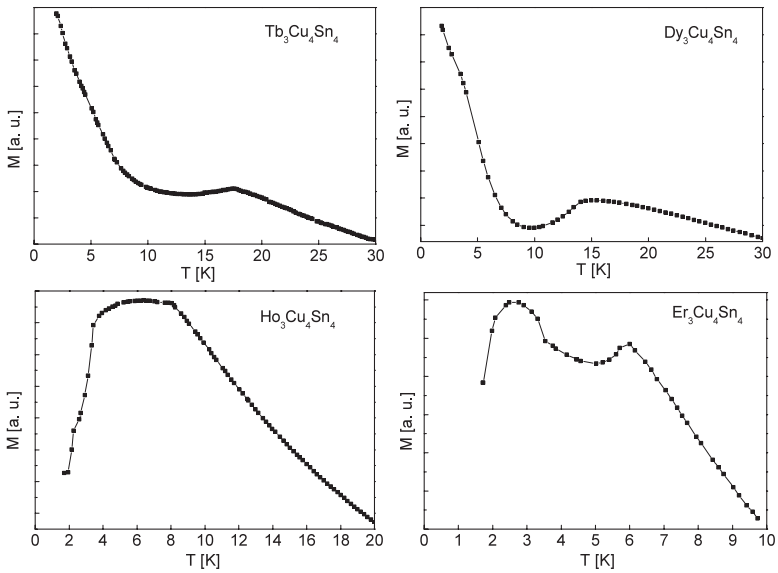

Figure 2. Temperature dependences of magnetization at the magnetic fields of 100 Oe for the $R_3Cu_4Sn_4$ (R = Tb, Dy, Ho, Er) compounds.

Table 2. The Néel temperatures T_N and the values of the magnetic moments μ of the $R_3Cu_4Sn_4$ (R = Tb, Dy, Ho, Er) compounds, determined from the magnetic (labelled by M) and the neutron diffraction (labelled by N) measurements. DMM stands for direction of the magnetic moment.

	T_N (K)		μ (μ_B)				
R	2d M	2d N	2d Exp	4e Exp	Theor	2d DMM	4e DMM
Tb	17.5	17.5	8.7(3)	6.8(2)	9.0	‖a	‖a
Dy	14	15	8.2(5)	7.3(3)	10.0	‖a	‖a
Ho	8		8.3(1)	10.0(1)	10.0	‖b	‖a
Er	6	6	6.9(1)	1.8(4)	9.0	‖c	‖c

4.2.1. $Tb_3Cu_4Sn_4$. The neutron diffraction patterns of $Tb_3Cu_4Sn_4$ observed at low temperatures are shown in figure 3. The Tb magnetic moments occupy two sites with the following positions in the crystal unit cell:

- 4e sites: M_1 $(x, 0, 0)$, M_2 $(1-x, 0, 0)$, M_3 $(\frac{1}{2}+x, \frac{1}{2}, \frac{1}{2})$ M_4 $(\frac{1}{2}-x, \frac{1}{2}, \frac{1}{2})$ and
- 2d sites: M_5 $(\frac{1}{2}, 0, \frac{1}{2})$, M_6 $(0, \frac{1}{2}, 0)$.

The analysis indicates that at 1.5 K the peaks of magnetic origin can be indexed with the propagation vector $\boldsymbol{k} = (0, 0, \frac{1}{2}+\delta)$, $\delta = 0.0848(2)$, $R_{mag} = 19.83\%$. For the $Immm$ space group, the propagation vector $\boldsymbol{k} = (0, 0, k_z)$ and the 2d position the symmetry analysis allows three one-dimensional representations, τ_2, τ_3, τ_4 [15], each of them appearing once. For the 4e positions four representations are allowed, two of them (τ_2, τ_3) once and two others (τ_1, τ_4) twice. The symmetry analysis calculations show, that in this case all possible orderings of magnetic structures in each sublattice, correspondingly in the x, y and z direction, may be done by one representation, and for each representation the model of the structure is completely fixed by two independent parameters (c^ν and Ψ^ν for the 4e sublattice and d^ν and Θ^ν for the 2d sublattice).

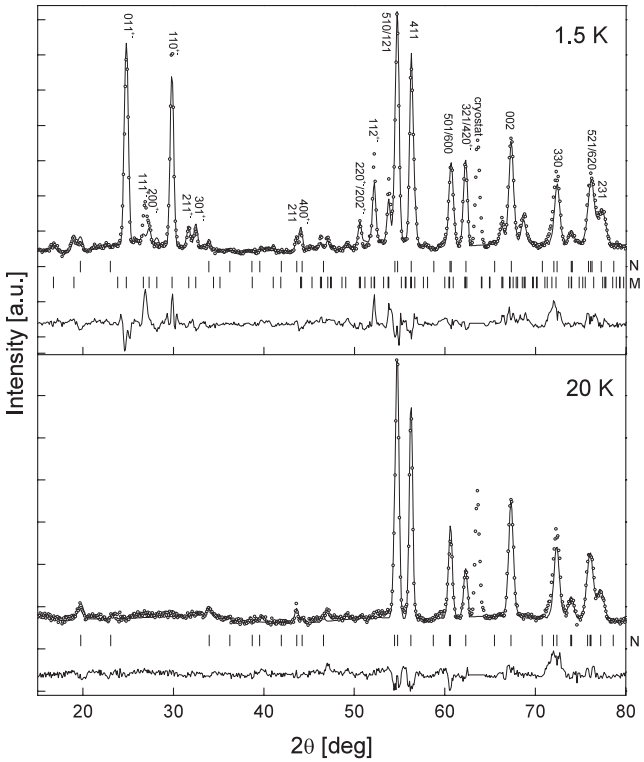

Figure 3. Neutron diffraction patterns of $Tb_3Cu_4Sn_4$ collected at 1.5 and 20 K. The dots represent the experimental points; the solid curves are calculated profiles for the model crystal and magnetic structures described in the text and the differences between the observed and calculated intensities (at the bottom of each diagram). The vertical bars indicate the Bragg peaks of nuclear (N) and magnetic (M) phases. One interval of 2θ is excluded owing to cryostat reflections.

The best fit to the experimental data gives the model in which the magnetic moments in both sublattices are parallel to the xz-plane and are collinear, but the directions of the ordering in the sublattices form a small angle. For both 2d and 4e sites the structure may be described as a linear combination of basis vectors of τ_3 (x-components) and τ_2 (z-components) irreducible representations (see tables 3, 4). For the 4e sites the parameters are $c^3 = 6.7\ \mu_B$, $c^2 = 1.6\ \mu_B$, $\Psi^3 = \Psi^2$. For the 2d sites the parameters are $d^3 = 8.6\ \mu_B$ and $d^2 = 1.2\ \mu_B$, $\Theta^3 = \Theta^2$. It is not possible to determine the absolute values of Θ^3 and Ψ^3 from the diffraction patterns of polycrystalline samples, but $\Phi = (\Theta^3 - \Psi^3) = -0.52\pi$. The resulting magnetic structure may be written as:

- for the 4e sublattice (with $k_z = 0.5848(2)$):

$$\boldsymbol{M}(1+\boldsymbol{t}) = \boldsymbol{M}(2+\boldsymbol{t}) = (c^3\boldsymbol{e}_x - c^2\boldsymbol{e}_z)\cos(\boldsymbol{kt} + \Psi^3)$$
$$\boldsymbol{M}(3+\boldsymbol{t}) = \boldsymbol{M}(4+\boldsymbol{t}) = (c^3\boldsymbol{e}_x - c^2\boldsymbol{e}_z)\cos(\boldsymbol{kt} + \pi k_z + \Psi^3)$$

- for the 2d sublattice

$$\boldsymbol{M}(5+\boldsymbol{t}) = (d^3\boldsymbol{e}_x + d^2\boldsymbol{e}_z)\cos(\boldsymbol{kt} + \Theta^3)$$
$$\boldsymbol{M}(6+\boldsymbol{t}) = (d^3\boldsymbol{e}_x + d^2\boldsymbol{e}_z)\cos(\boldsymbol{kt} - \pi k_x + \Theta^3)$$

Table 3. Basic vectors of the irreducible representations for $\boldsymbol{k} = (0, 0, k_z)$ of the $Immm$ space group in the 2d positions; $\varphi = \pi k_z$.

	$(\frac{1}{2}, 0, \frac{1}{2})$	$(0, \frac{1}{2}, 0)$
	$\boldsymbol{k}$	
τ_2	$(0, 0, 1)$	$(0, 0, e^{-i\varphi})$
τ_3	$(1, 0, 0)$	$(e^{-i\varphi}, 0, 0)$
τ_4	$(0, 1, 0)$	$(0, e^{-i\varphi}, 0)$
	$-\boldsymbol{k}$	
τ_2	$(0, 0, -e^{-2i\varphi})$	$(0, 0, -e^{-i\varphi})$
τ_3	$(e^{-2i\varphi}, 0, 0)$	$(e^{-i\varphi}, 0, 0)$
τ_4	$(0, -e^{-2i\varphi}, 0)$	$(0, -e^{-i\varphi}, 0)$

Table 4. Basic vectors of the irreducible representations for $\boldsymbol{k} = (0, 0, k_z)$ of the $Immm$ space group in the 4e positions; $\varphi = \pi k_z$.

	$(x, 0, 0)$	$(1 - x, 0, 0)$	$(x + \frac{1}{2}, \frac{1}{2}, \frac{1}{2})$	$(\frac{1}{2} - x, \frac{1}{2}, \frac{1}{2})$
			$\boldsymbol{k}$	
τ_1	$(0, 1, 0)$	$(0, -1, 0)$	$(0, e^{i\varphi}, 0)$	$(0, -e^{i\varphi}, 0)$
τ_2	$(1, 0, 0)$	$(-1, 0, 0)$	$(e^{i\varphi}, 0, 0)$	$(-e^{i\phi}, 0, 0)$
τ_2'	$(0, 0, 1)$	$(0, 0, 1)$	$(0, 0, e^{i\varphi})$	$(0, 0, e^{i\varphi})$
τ_3	$(1, 0, 0)$	$(1, 0, 0)$	$(e^{i\varphi}, 0, 0)$	$(e^{i\varphi}, 0, 0)$
τ_3'	$(0, 0, 1)$	$(0, 0, -1)$	$(0, 0, e^{i\varphi})$	$(0, 0, -e^{i\varphi})$
τ_4	$(0, 1, 0)$	$(0, 1, 0)$	$(0, e^{i\varphi}, 0)$	$(0, e^{i\varphi}, 0)$
			$-\boldsymbol{k}$	
τ_1	$(0, -1, 0)$	$(0, 1, 0)$	$(0, -e^{-i\varphi}, 0)$	$(0, e^{-i\varphi}, 0)$
τ_2	$(1, 0, 0)$	$(-1, 0, 0)$	$(e^{-i\varphi}, 0, 0)$	$(-e^{-i\varphi}, 0, 0)$
τ_2'	$(0, 0, -1)$	$(0, 0, -1)$	$(0, 0, -e^{-i\varphi})$	$(0, 0, -e^{-i\varphi})$
τ_3	$(1, 0, 0)$	$(1, 0, 0)$	$(e^{-i\varphi}, 0, 0)$	$(e^{-i\varphi}, 0, 0)$
τ_3'	$(0, 0, -1)$	$(0, 0, 1)$	$(0, 0, -e^{-i\varphi})$	$(0, 0, e^{-i\phi})$
τ_4	$(0, -1, 0)$	$(0, -1, 0)$	$(0, -e^{-i\varphi}, 0)$	$(0, -e^{-i\varphi}, 0)$

The temperature dependences of the intensities of the $011^{\pm}$, $110^{\pm}$ and $112^{\pm}$ reflections, the values of the magnetic moments and the δ value are shown in figure 4 (in (b), (c) and (d) respectively). These dependences, in particular from figures 4(b) and (c), indicate that the magnetic ordering in both sublattices disappears simultaneously at about 17.5 K. The moment values in general decrease with increasing temperature (see figure 4(c)). The 2d sublattice moment is at all temperatures bigger than the one in the 4e sites and neither changes its orientation (along a direction, mutually antiparallel). The δ value increases (when we exclude its value at 17 K from the considerations, see figure 4(d)) with increasing temperature. The Tb magnetic moments disorder at a Néel temperature of about 17.5 K.

4.2.2. $Dy_3Cu_4Sn_4$. In the neutron diffraction pattern of $Dy_3Cu_4Sn_4$ at 1.5 K the additional peaks of magnetic origin are observed (figure 5).

The analysis of the magnetic peak intensities indicates that at 1.5 K the magnetic peaks can be indexed with the propagation vector $\boldsymbol{k} = (0, 0, \frac{1}{2} + \delta)$ where δ is equal to 0.0851(4), $R_{\mathrm{mag}} = 21.86\%$. The Dy moments order similarly as in the case of $Tb_3Cu_4Sn_4$ (they form

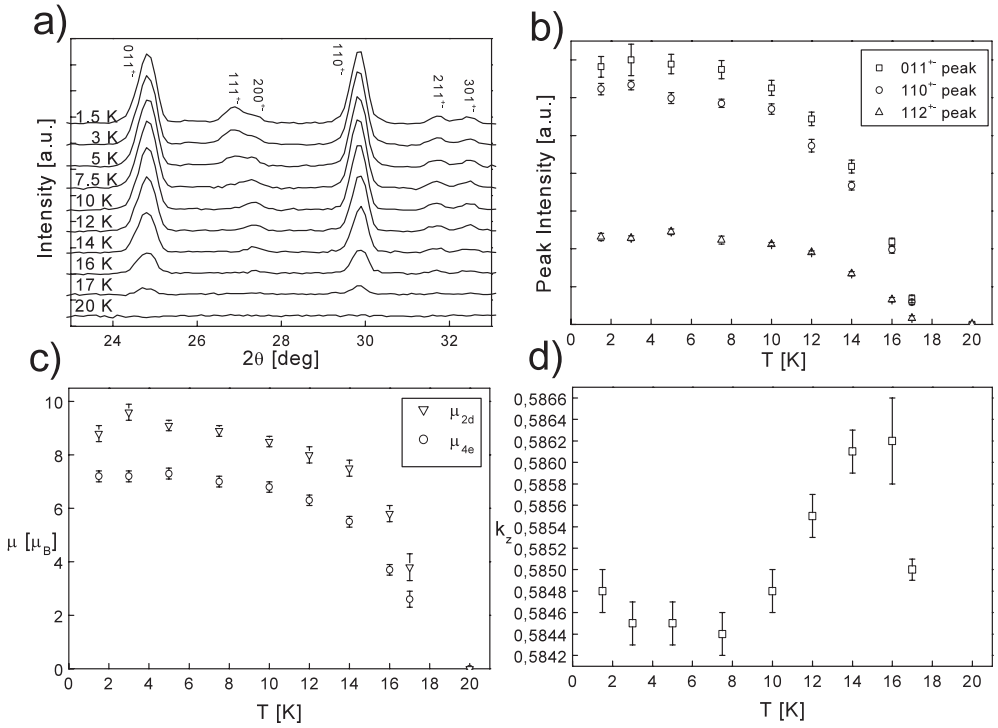

Figure 4. Part of the neutron diffraction patterns of $Tb_3Cu_4Sn_4$ measured as a function of temperature (a) and the temperature dependences of the magnetic peaks intensities (b), magnetic moment values (c) and the $k_z = \frac{1}{2} + \delta$ value (d).

the modulated structure in the xz-plane). The structure may also be described as a linear combination of basis vectors of τ_3 (x-components) and τ_2 (z-components) irreducible representations. The difference is for the 2d sites, where only the x-components are non-zero, and for the 4e sites, where the x and z components both have the same sign. The parameters which give the best fit of the model to the experimental data are $c_x^3 = 6.4\ \mu_B$, $c_z^2 = 3.4\ \mu_B$, $d_x^3 = 8.2\ \mu_B$, $\Phi = (\Theta^3 - \Psi^3) = -0.51\pi$.

The magnetic moments in both 4e and 2d sites order in one crystallographic cell ferromagnetically. The moment values are 8.2(5) μ_B and 7.3(3) μ_B for the 2d and 4e sublattices respectively. The temperature dependence of the intensities of the $011^{\pm}$ and $110^{\pm}$ reflections is shown in figure 6(b). It reveals that the Dy magnetic moments remain ordered up to the Néel temperature of about 15 K. The magnetic peaks positions, which do not change with increasing temperature (see figure 6(a)), suggest that the magnetic structure does not change either.

4.2.3. $Ho_3Cu_4Sn_4$. The $Ho_3Cu_4Sn_4$ magnetic structure, resulting in additional peaks in the neutron diffraction pattern, is observed at low temperatures (see figure 7). The way of ordering is more complicated in comparison to the two previously described cases.

The analysis reveals that at 1.5 K the magnetic peaks can be indexed with two propagation vectors: $\boldsymbol{k}_1 = (0.364(2), \frac{1}{2}, \frac{1}{2})$ for the 4e sublattice ($R_{mag} = 17.67\%$) and $\boldsymbol{k}_2 = (0, \frac{1}{2}, 0)$ for the 2d sublattice ($R_{mag} = 18.03\%$). For the $Immm$ space group, and the propagation vector $\boldsymbol{k}_1 = (0.364(2), \frac{1}{2}, \frac{1}{2})$, the 4e sublattice splits into two orbits in the $G(k)$ group (positions 1

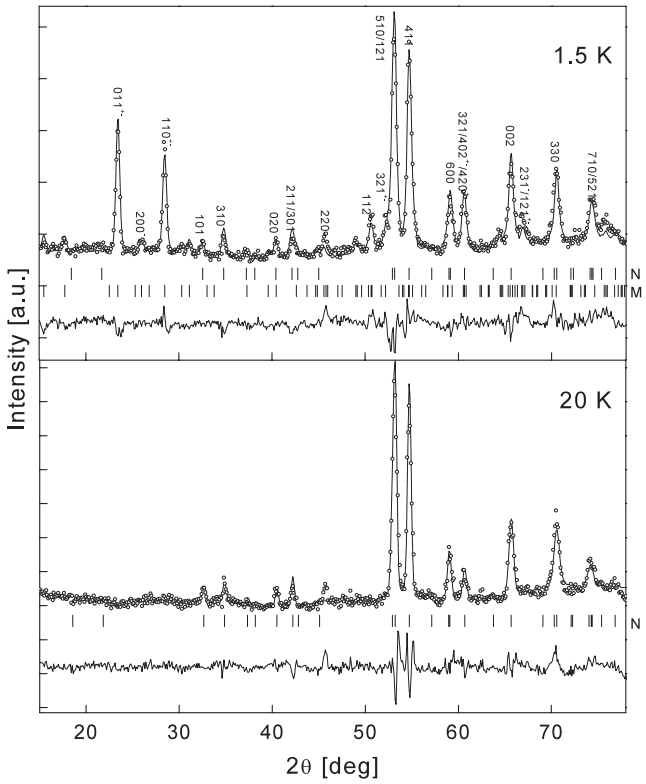

Figure 5. Neutron diffraction patterns of $Dy_3Cu_4Sn_4$ collected at 1.5 and 20 K. The dots represent the experimental points; the solid curves are calculated profiles for the model crystal and magnetic structures described in the text and the differences between the observed and calculated intensities (at the bottom of each diagram). The vertical bars indicate the Bragg peaks of nuclear (N) and magnetic (M) phases. A small amount of an impurity (most probably SnO_2) is present (peak at about 46°).

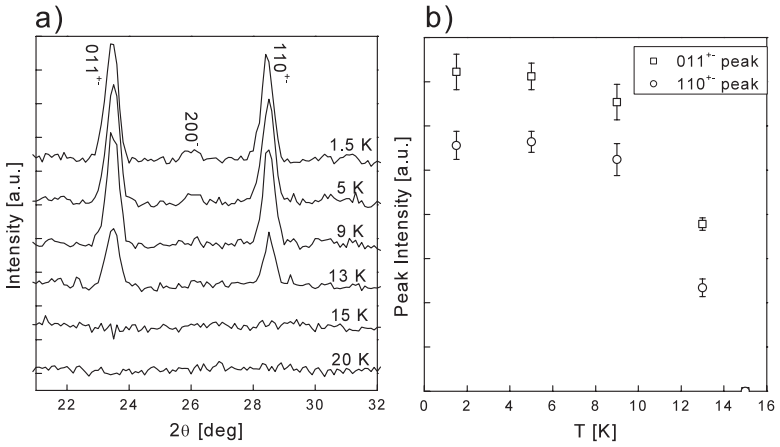

Figure 6. The part of the neutron diffraction patterns of $Dy_3Cu_4Sn_4$ measured as a function of temperature (a) and the temperature dependence of the magnetic peaks intensities (b).

and 3 belong to the first orbit and positions 2 and 4 belong to the second orbit). For each orbit the symmetry analysis allows two one-dimensional representations: τ_1, appearing once, and τ_2, appearing twice (see table 5). The symmetry analysis calculations show that all possible models of the magnetic structure in this sublattice may be obtained for each representation and each orbit by two independent parameters, c_i^ν and Ψ_i^ν (where i is the number of the orbit). As regards the 2d sublattice and the $\boldsymbol{k}_2$ propagation vector, three one-dimensional, complex representations, τ_2, τ_3 and τ_4, each of them appearing once, are allowed (see table 6). The best fit to the experimental data gives the model in which the magnetic moments are aligned along the x-direction in the 4e sublattice (described by the basis vectors of τ_1 with the parameters $c_1^1 = c_2^1$, $\Psi_1^1 = \Psi_2^1$) and along the y-direction in the 2d sites (described by the basis vectors of physical representation $\tau_2 + \tau_2^*$ with the parameters d^2, θ^2). The resulting magnetic structure may be written as:

- for the 4e sublattice:

$$\boldsymbol{M}(1+\boldsymbol{t}) = \boldsymbol{M}(2+\boldsymbol{t}) = c^1 \boldsymbol{e}_x \cos(\boldsymbol{kt} + \Psi^1)$$
$$\boldsymbol{M}(3+\boldsymbol{t}) = \boldsymbol{M}(4+\boldsymbol{t}) = -c^1 \boldsymbol{e}_x \cos(\boldsymbol{kt} + \pi k_x + \Psi^1)$$

  ($k_x = 0.364$, Ψ^1 not determined from powder diffraction pattern).
- for the 2d sublattice:

$$\boldsymbol{M}(5+\boldsymbol{t}) = d^2 \boldsymbol{e}_y \cos(\boldsymbol{kt} + \theta^2)$$
$$\boldsymbol{M}(6+\boldsymbol{t}) = d^2 \boldsymbol{e}_y \cos\left(\boldsymbol{kt} + \frac{\pi}{2} + \theta^2\right)$$

  where $\theta^2 = \Psi^1$.

As can be seen, the Ho magnetic moments in the 4e sublattice form an antiferromagnetic order with the sequence of signs $++--$ in the space of the crystal unit cell; $c^1 = \mu_{4e} = 10.0(1)\ \mu_B$. In the 2d sublattice the Ho magnetic moments form a ferromagnetic order in the space of the crystal unit cell; $d^2 = \mu_{2d} = 8.3(1)\ \mu_B$.

At 2.5 K the way of ordering does not change although the values of the magnetic moments and the x-component of the $\boldsymbol{k}_1$ vector do: $\boldsymbol{k}_1 = (0.332(3), \frac{1}{2}, \frac{1}{2})$, $\mu_{4e} = 8.8(1)\ \mu_B$ ($R_{mag} = 17.76\%$), and $\mu_{2d} = 8.3(1)\ \mu_B$ ($R_{mag} = 18.72\%$), both oriented as they were previously.

At 3 K the way of ordering in the 2d sublattice does not change, $\mu_{2d} = 8.2(1)\ \mu_B$ along the b-axis ($R_{mag} = 19.25\%$) but the $\boldsymbol{k}_1$ vector changes significantly. Now $\boldsymbol{k}_1 = (\frac{1}{2}, \frac{1}{2}, 0.4685(3))$ ($R_{mag} = 19.74\%$). For the $Immm$ space group, the $\boldsymbol{k}_1$ vector and the 4e sublattice the symmetry analysis allows two one-dimensional representations: τ_1 and τ_2, both appearing three times (see table 7). The best fit to the experimental data gives the model in which the Ho magnetic moments in the 4e sublattice form a modulated structure with antiferromagnetic order with the sequence of signs $+--\,--$ in the space of the crystal unit cell, $\mu_{4e} = 7.7(1)\ \mu_B$, (still along the a-axis), described by the basis vectors of τ_2.

At 6.5 K the magnetic structure is described by only one propagation vector which seems to be a modification of the $\boldsymbol{k}_2$ vector and describes the magnetic ordering in both sublattices. Now $\boldsymbol{k}_2 = (0.069(2), 0.480(1), 0)$ ($R_{mag} = 22.05\%$). In this case, similar to 1.5 K, the 4e sublattice splits into two orbits in the $G(\boldsymbol{k})$ group (positions 1 and 3 belong to the first orbit and positions 2 and 4 belong to the second orbit), while the 2d positions form one orbit in $G(\boldsymbol{k})$. For the 2d sublattice and both orbits of the 4e sublattice the symmetry analysis allows two one-dimensional representations: τ_1, appearing once, and τ_2, appearing twice (see tables 8 and 9). The symmetry analysis calculations and their results in this case are similar to those for 1.5 K. The analysis of the diffraction pattern leads to the modulated structure with the directions of

Table 5. Basic vectors of the irreducible representations for $\boldsymbol{k} = (k_x, \frac{1}{2}, \frac{1}{2})$ of the $Immm$ space group in the 4e positions; $\varphi = \pi k_x$.

		$(x, 0, 0)$	$(1-x, 0, 0)$	$(x+\frac{1}{2}, \frac{1}{2}, \frac{1}{2})$	$(\frac{1}{2}-x, \frac{1}{2}, \frac{1}{2})$
			$\boldsymbol{k}$		
τ_1	1st orbit	$(1, 0, 0)$		$(-e^{i\varphi}, 0, 0)$	
	2nd orbit		$(1, 0, 0)$		$(-e^{-i\varphi}, 0, 0)$
τ_2	1st orbit	$(0, 1, 0)$		$(0, -e^{i\varphi}, 0)$	
	2nd orbit		$(0, 1, 0)$		$(0, -e^{-i\varphi}, 0)$
τ_2'	1st orbit	$(0, 0, 1)$		$(0, 0, -e^{i\varphi})$	
	2nd orbit		$(0, 0, 1)$		$(0, 0, -e^{-i\varphi})$
			$-\boldsymbol{k}$		
τ_1	1st orbit	$(e^{-2i\varphi}, 0, 0)$		$(-e^{-3i\varphi}, 0, 0)$	
	2nd orbit		$(e^{-2i\varphi}, 0, 0)$		$(-e^{-i\varphi}, 0, 0)$
τ_2	1st orbit	$(0, e^{-2i\varphi}, 0)$		$(0, -e^{-3i\varphi}, 0)$	
	2nd orbit		$(0, e^{-2i\varphi}, 0)$		$(0, -e^{-i\varphi}, 0)$
τ_2'	1st orbit	$(0, 0, e^{-2i\varphi})$		$(0, 0, -e^{-3i\varphi})$	
	2nd orbit		$(0, 0, e^{-2i\varphi})$		$(0, 0, -e^{-i\varphi})$

the moments the same as at 1.5 K—in the 4e sublattice along the a-axis (described by the basis vectors of τ_2 with the parameters $c_1^2 = c_2^2 = c^2$) and in the 2d sites along the b-axis (described by the basis vectors of the τ_2' representation, with the parameters d^2 and θ^2). The resulting magnetic structure for the 4e sublattice may be written as:

- for the first orbit:

$$\boldsymbol{M}(1+\boldsymbol{t}) = c^2\boldsymbol{e_x}\cos(\boldsymbol{kt} + \Psi_1^2)$$
$$\boldsymbol{M}(3+\boldsymbol{t}) = c^2\boldsymbol{e_x}\cos(\boldsymbol{kt} + \pi(k_x + k_y) + \Psi_1^2)$$

- for the second orbit:

$$\boldsymbol{M}(2+\boldsymbol{t}) = c^2\boldsymbol{e_x}\cos(\boldsymbol{kt} + \Psi_2^2)$$
$$\boldsymbol{M}(4+\boldsymbol{t}) = c^2\boldsymbol{e_x}\cos(\boldsymbol{kt} + \pi(-k_x + k_y) + \Psi_2^2)$$

  (Ψ^2 is not determined from powder diffraction pattern)

- for the 2d sublattice:

$$\boldsymbol{M}(5+\boldsymbol{t}) = (b^2\boldsymbol{e_x} + d^2\boldsymbol{e_y})\cos(\boldsymbol{kt} + \theta^2)$$
$$\boldsymbol{M}(6+\boldsymbol{t}) = (b^2\boldsymbol{e_x} + d^2\boldsymbol{e_y})\cos(\boldsymbol{kt} + \pi(-k_x + k_y) + \theta^2).$$

Magnetic moment values are as follows: $d^2 = \mu_{y2d} = 7.9(3)\,\mu_B$, $b^2 = \mu_{x2d} = 1.7(3)\,\mu_B$, $c^2 = \mu_{4e} = 3.3(3)\,\mu_B$, $\Psi_1^2 = \theta^2$. A small difference between Ψ_1^2 and Ψ_2^2 appears. For this space group, propagation vector and sublattices the symmetry analysis allows two one-dimensional representations: τ_1 and τ_2, both appearing three times (see tables 8 and 9). The best fit to the experimental data gives the model in which the magnetic moments ordering in both sublattices is described by the basis vectors of τ_2.

At 15 K the Ho moments are no longer ordered.

The diffraction patterns of $Ho_3Cu_4Sn_4$ for 2θ ranging from 10° to 25° and for temperatures between 1.5 and 15 K are collected in figure 8. Constant changes of angular positions of the magnetic peaks are observed. This makes one aware of how complicated the structure is.

Table 6. Basic vectors of the irreducible representations for $\boldsymbol{k} = (0, \frac{1}{2}, 0)$ of the $Immm$ space group in the 2d positions.

	$(\frac{1}{2}, 0, \frac{1}{2})$	$(0, \frac{1}{2}, 0)$
τ_2	(0, 1, 0)	(0, i, 0)
τ_3	(1, 0, 0)	(i, 0, 0)
τ_4	(0, 0, 1)	(0, 0, i)

Table 7. Basic vectors of the irreducible representations for $\boldsymbol{k} = (\frac{1}{2}, \frac{1}{2}, k_z)$ of the $Immm$ space group in the 4e positions; $\varphi = \pi k_z$.

	$(x, 0, 0)$	$(1-x, 0, 0)$	$(x+\frac{1}{2}, \frac{1}{2}, \frac{1}{2})$	$(\frac{1}{2}-x, \frac{1}{2}, \frac{1}{2})$
			$\boldsymbol{k}$	
τ_1	(1, 0, 0)	(1, 0, 0)	$(-e^{i\varphi}, 0, 0)$	$(e^{i\varphi}, 0, 0)$
τ_1'	(0, 1, 0)	(0, 1, 0)	$(0, -e^{i\varphi}, 0)$	$(0, e^{i\varphi}, 0)$
τ_1''	(0, 0, 1)	(0, 0, −1)	$(0, 0, -e^{i\varphi})$	$(0, 0, -e^{i\varphi})$
τ_2	(1, 0, 0)	(−1, 0, 0)	$(-e^{i\varphi}, 0, 0)$	$(-e^{i\varphi}, 0, 0)$
τ_2'	(0, 1, 0)	(0, −1, 0)	$(0, -e^{i\varphi}, 0)$	$(0, -e^{i\varphi}, 0)$
τ_2''	(0, 0, 1)	(0, 0, 1)	$(0, 0, -e^{i\varphi})$	$(0, 0, e^{i\varphi})$
			$-\boldsymbol{k}$	
τ_1	(−1, 0, 0)	(−1, 0, 0)	$(-e^{-i\varphi}, 0, 0)$	$(-e^{-i\phi}, 0, 0)$
τ_1'	(0, −1, 0)	(0, −1, 0)	$(0, e^{-i\varphi}, 0)$	$(0, -e^{-i\varphi}, 0)$
τ_1''	(0, 0, 1)	(0, 0, −1)	$(0, 0, -e^{-i\varphi})$	$(0, 0, -e^{-i\varphi})$
τ_2	(1, 0, 0)	(−1, 0, 0)	$(-e^{-i\varphi}, 0, 0)$	$(-e^{-i\varphi}, 0, 0)$
τ_2'	(0, 1, 0)	(0, −1, 0)	$(0, -e^{-i\varphi}, 0)$	$(0, -e^{-i\varphi}, 0)$
τ_2''	(0, 0, −1)	(0, 0, −1)	$(0, 0, e^{-i\varphi})$	$(0, 0, -e^{-i\varphi})$

Table 8. Basic vectors of the irreducible representations for $\boldsymbol{k} = (k_x, k_y, 0)$ of the $Immm$ space group in the 2d positions; $\varphi = \pi(k_x + k_y)$, $\psi = 2\pi k_x$.

	$(\frac{1}{2}, 0, \frac{1}{2})$	$(0, \frac{1}{2}, 0)$
	$\boldsymbol{k}$	
τ_1	(0, 0, 1)	$(0, 0, e^{i(\varphi-\psi)})$
τ_2	(1, 0, 0)	$(e^{i(\varphi-\psi)}, 0, 0)$
τ_2'	(0, 1, 0)	$(0, e^{i(\varphi-\psi)}, 0)$
	$-\boldsymbol{k}$	
τ_1	$(0, 0, e^{-i\psi})$	$(0, 0, e^{-i\varphi})$
τ_2	$(-e^{-i\psi}, 0, 0)$	$(-e^{-i\varphi}, 0, 0)$
τ_2'	$(0, -e^{-i\psi}, 0)$	$(0, -e^{-i\varphi}, 0)$

4.2.4. $Er_3Cu_4Sn_4$. In the neutron diffraction pattern of $Er_3Cu_4Sn_4$ at 1.5 K additional peaks of magnetic origin are observed (figure 9). The ordering of the Er magnetic moments at low temperatures is described by two propagation vectors.

The analysis indicates that at 1.5 K the magnetic peaks can be indexed with two propagation vectors: $\boldsymbol{k}_1 = (\frac{1}{2}, \frac{1}{2}, 0)$ which describes the ordering in the 2d sublattice ($R_{\mathrm{mag}} = 21.61\%$) and $\boldsymbol{k}_2 = (0, 0, \delta)$ where $\delta = 0.08(2)$ which describes the ordering in the 4e sublattice ($R_{\mathrm{mag}} = 22.99\%$). The Er moments in both sublattices form a modulated structure with ferromagnetic order in the space of one crystallographic cell. The Er moments in both

Table 9. Basic vectors of the irreducible representations for $\boldsymbol{k} = (k_x, k_y, 0)$ of the $Immm$ space group in the 4e positions; $\varphi = \pi(k_x + k_y)$, $\psi = 2\pi k_x$.

		$(x, 0, 0)$	$(1-x, 0, 0)$	$(x+\frac{1}{2}, \frac{1}{2}, \frac{1}{2})$	$(\frac{1}{2}-x, \frac{1}{2})$
			$\boldsymbol{k}$		
τ_1	1st orbit	$(0, 0, 1)$		$(0, 0, e^{i\varphi})$	
	2nd orbit		$(0, 0, 1)$		$(0, 0, e^{i(\varphi-\psi)})$
τ_2	1st orbit	$(1, 0, 0)$		$(e^{i\varphi}, 0, 0)$	
	2nd orbit		$(1, 0, 0)$		$(e^{i(\varphi-\psi)}, 0, 0)$
τ_2'	1st orbit	$(0, 1, 0)$		$(0, e^{i\varphi}, 0)$	
	2nd orbit		$(0, 1, 0)$		$(0, e^{i(\varphi-\psi)}, 0)$
			$-\boldsymbol{k}$		
τ_1	1st orbit	$(0, 0, e^{-i\psi})$		$(0, 0, e^{-i(\varphi+\psi)})$	
	2nd orbit		$(0, 0, e^{-i\psi})$		$(0, 0, e^{-i\varphi})$
τ_2	1st orbit	$(-e^{-i\psi}, 0, 0)$		$(-e^{-i(\varphi+\psi)}, 0, 0)$	
	2nd orbit		$(-e^{-i\psi}, 0, 0)$		$(-e^{-i\varphi}, 0, 0)$
τ_2'	1s orbit	$(0, -e^{-i\psi}, 0)$		$(0, -e^{-i(\varphi+\psi)}, 0)$	
	2nd orbit		$(0, -e^{-i\psi}, 0)$		$(0, -e^{-i\varphi}, 0)$

Table 10. Basic vectors of the irreducible representations for $\boldsymbol{k} = (\frac{1}{2}, \frac{1}{2}, 0)$ of the $Immm$ space group in the 2d positions.

	$(\frac{1}{2}, 0, \frac{1}{2})$	$(0, \frac{1}{2}, 0)$
τ_2	$(1, 0, 0)$	$(1, 0, 0)$
τ_2'	$(0, 1, 0)$	$(0, 1, 0)$
τ_4	$(0, 0, 1)$	$(0, 0, 1)$

sublattices are aligned along the c-axis. The moment values are 6.9(1) μ_B and 1.8(4) μ_B for the 2d and 4e sublattices respectively. For the $Immm$ space group, the propagation vector $\boldsymbol{k}_1 = (\frac{1}{2}, \frac{1}{2}, 0)$ and the 2d position the symmetry analysis allows two one-dimensional representations: τ_2, appearing twice and τ_4, appearing once (see table 10). The best fit to the experimental data gives the model described by the basis vectors of τ_4. For the 4e positions and $\boldsymbol{k}_2 = (0, 0, \delta)$ the best fit to the experimental data gives the model which may be described by the basis vectors of the representation τ_2' (see table 4). The resulting magnetic structure may be written as:

$$\boldsymbol{M}(1+\boldsymbol{t}) = \boldsymbol{M}(2+\boldsymbol{t}) = c^{2'}\boldsymbol{e}_z \cos(\boldsymbol{kt} + \Psi^{2'})$$
$$\boldsymbol{M}(3+\boldsymbol{t}) = \boldsymbol{M}(4+\boldsymbol{t}) = c^{2'}\boldsymbol{e}_z \cos(\boldsymbol{kt} + \pi k_z + \Psi^{2'})$$

where $k_z = 0.08$.

At the higher temperature of 3.5 K only the 2d sublattice remains ordered, the $\boldsymbol{k}_1$ vector does not change but the 2d magnetic moment value equals 7.5(1) μ_B now ($R_{mag} = 33.01\%$).

At 6 K the Er magnetic moments are not ordered.

The diffraction patterns of $Er_3Cu_4Sn_4$ for 2θ ranging from 7° to 27° and for temperatures between 1.5 and 6.5 K are collected in figure 10(a) and the temperature dependence of the magnetic $100_2^{\pm}$ and 100_1^{+} peak intensities are in figure 10(b). One can observe that this dependence is anomalous—the magnetic peak intensities first increase to approach a maximum at about 3.3 K and then decrease with the increase of temperature.

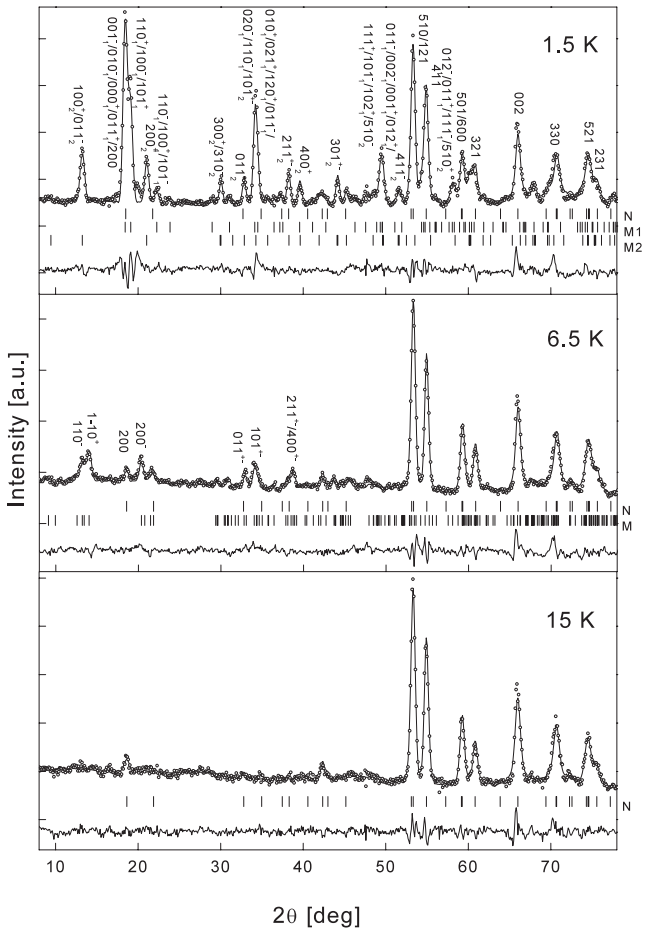

Figure 7. Neutron diffraction patterns of $Ho_3Cu_4Sn_4$ collected at 1.5, 6.5 and 15 K. The dots represent the experimental points; the solid curves are calculated profiles for the model crystal and magnetic structures described in the text and the differences between the observed and calculated intensities (at the bottom of each diagram). The vertical bars indicate the Bragg peaks of nuclear (N) and magnetic phases (M1 and M2 in the top diagram stand for the two magnetic phases described by the $\boldsymbol{k}_1$ and $\boldsymbol{k}_2$ propagation vectors, respectively, whereas M in the middle diagram indicates the Bragg reflections connected with the $\boldsymbol{k}_2$ vector).

5. Discussion

The results obtained in this investigation show that the $R_3Cu_4Sn_4$, where R = Tb, Dy, Ho and Er, compounds have complex magnetic properties. All of them crystallize in the orthorhombic $Gd_3Cu_4Ge_4$-type structure. Rare earth atoms occupy two non-equivalent 2d and 4e crystallographic positions. At low temperatures all these compounds order antiferromagnetically with different temperature dependences of the magnetic orderings.

$Tb_3Cu_4Sn_4$ and $Dy_3Cu_4Sn_4$ have similar magnetic structures, described by the propagation vector $\boldsymbol{k} = (0, 0, \frac{1}{2} + \delta)$. The rare earth moments in both 2d and 4e sites order at the same temperature and the resulting ordering is stable in the temperature range 1.5 K—T_N. The value of the Tb moment in the 2d site is close to the free Tb^{3+} ion value (9.0(3) μ_B) whereas in the 4e site it is smaller (only 6.8(2) μ_B). These moments lie in the a–c plane and form the angles of 8° (the 2d sublattice) and 13° (the 4e sublattice) with the a-axis.

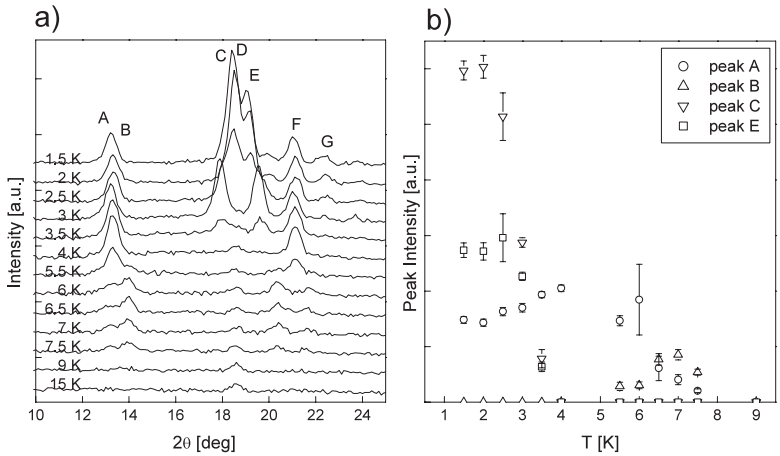

Figure 8. Part of the neutron diffraction patterns of $Ho_3Cu_4Sn_4$ measured as a function of temperature (a) and the temperature dependence of the magnetic peaks intensities (b). A, B, C, D, E, F and G indicate the $100_2^+/010_2^-$, 110^-, $001_1^-/010_1^-/000_1^+/011_1^+$, 200, $110_1^+/100_1^-/101_1^+$, 200_2^+ and $110_1^-/100_1^+/101_1^-$ peaks.

In $Dy_3Cu_4Sn_4$ the Dy magnetic moment is equal to 8.2(5) μ_B in the 2d and 7.3(3) μ_B in the 4e sites and is parallel to the a-axis or forms an angle of 27.5° with the a-axis respectively.

Totally different and complex magnetic ordering is observed in $Ho_3Cu_4Sn_4$. At a temperature of 1.5 K the Ho moment equals 8.3(1) μ_B in the 2d and 10.0(1) μ_B in the 4e sites and is parallel to the b- and a-axis respectively. With increasing temperature a change in the magnetic structure is observed.

In $Er_3Cu_4Sn_4$ the Er moment is equal to 6.9(1) μ_B in the 2d and 1.8(4) μ_B in the 4e sites and is parallel to the c-axis in both sublattices. With increasing temperature the Er moment in the 4e sites disappears. In our measurements we did not detect a phase transition observed near the Néel temperature at $T_1 = 5.6$ K in [9]. The forms of the propagation vectors are consistent with ours.

The magnetic properties including magnetic structures of the intermetallic rare earth compounds result from competition between the Ruderman–Kittel–Kasuya–Yosida (RKKY) interactions, the magnetocrystalline anisotropy caused by the influence of the crystal electric field (CEF) and the magnetostriction effect. The long-range RKKY exchange interactions mediated by conduction electrons favour long-range magnetic ordering while the magnetocrystalline anisotropy favours uniaxial magnetic ordering.

In the RKKY model the Néel temperatures T_N are proportional to the de Gennes factor $G = (g_J - 1)^2 J(J + 1)$ [16]. According to this scaling T_N should have a maximum for $Gd_3Cu_4Ge_4$. For the investigated compounds the Néel temperatures do not satisfy the de Gennes relation (see figure 11). This result shows that a simple RKKY model is not suitable for the description of the magnetic properties of these compounds. This interaction is necessarily modified by the crystalline electric field effect or magnetostriction, which can significantly influence the magnitude of the Néel temperature [17].

The second factor which influences the magnetic ordering is crystal electric field. In the orthorhombic $Gd_3Cu_4Ge_4$-type ($Immm$ space group) crystal structure the rare earth atoms occupy two non-equivalent sites: 2d with the $2mm$ symmetry and 4e with the mmm symmetry. The magnetic behaviour is different in these two sites, namely, except for the Ho compound, the magnetic moment in the high-symmetry site is larger than the one in the low-symmetry site.

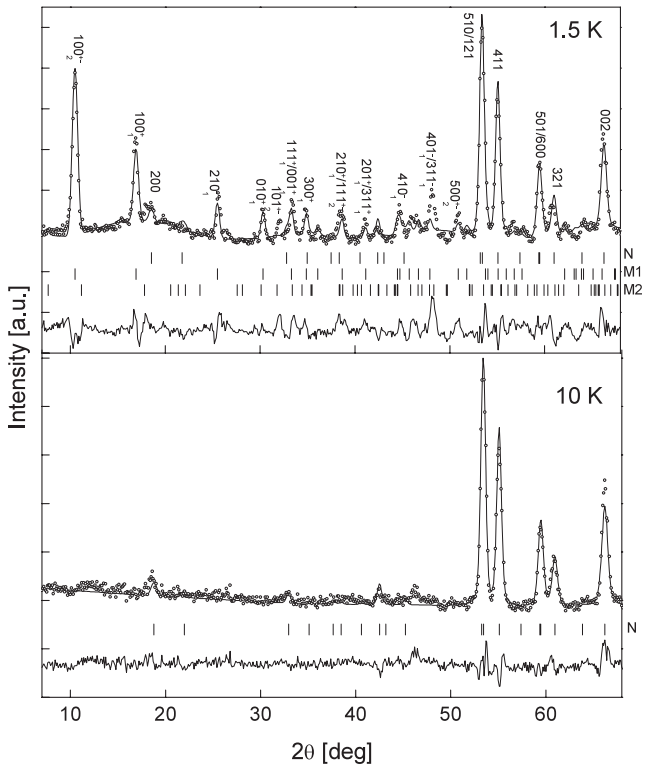

Figure 9. Neutron diffraction patterns of $Er_3Cu_4Sn_4$ collected at 1.5 and 10 K. The dots represent the experimental points; the solid curves are calculated profiles for the model crystal and magnetic structures described in the text and the differences between the observed and calculated intensities (at the bottom of each diagram). The vertical bars indicate the Bragg peaks of nuclear (N) and magnetic (M1 and M2 for the $\boldsymbol{k}_1$ and $\boldsymbol{k}_2$ propagation vectors respectively) phases. The indices 1 and 2 label the magnetic peaks connected with the propagation vectors $\boldsymbol{k}_1$ and $\boldsymbol{k}_2$ respectively. A small amount of impurity (most probably SnO_2) is present (peak at about 46°).

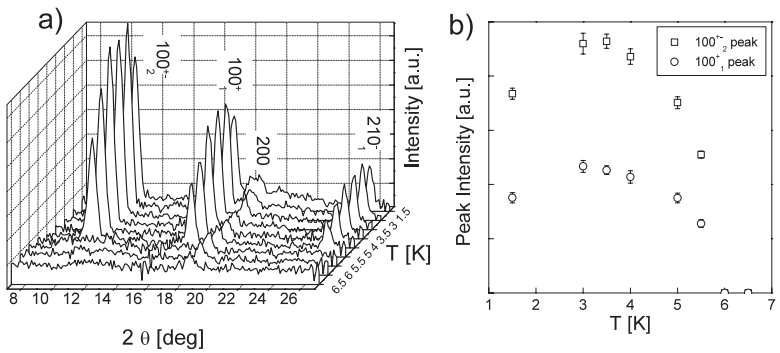

Figure 10. Part of the neutron diffraction patterns of $Er_3Cu_4Sn_4$ measured as a function of temperature (a) and the temperature dependence of the magnetic peak intensities (b). The indices 1 and 2 label the magnetic peaks connected with the propagation vectors $\boldsymbol{k}_1$ and $\boldsymbol{k}_2$ respectively.

It is likely that the moment reduction is caused by the CEF behaviour. The observed deviation of the magnetic moments from the a-axis for the Tb and Er compounds and their alignment

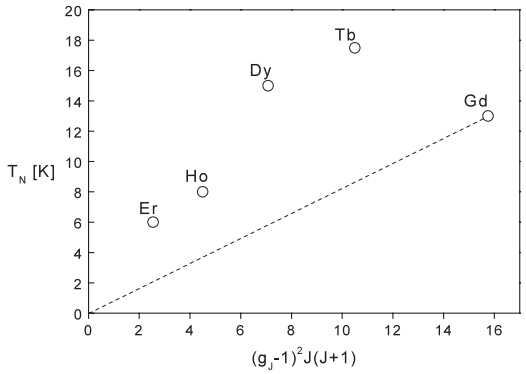

Figure 11. The Néel temperatures versus the de Gennes function for the $R_3Cu_4Sn_4$ (R = Tb, Dy, Ho and Er) compounds. The Néel temperature for Gd was taken from [6].

in the *b–c* plane for the Ho and Er compounds is due to the evolution of the parameters of the CEF with the increase of the number of the 4f electrons.

The evolution of the magnetic ordering in $Ho_3Cu_4Sn_4$ is in good agreement with the mean-field model of magnetic systems, which takes into account the periodic exchange of field and CEF effect [18].

Disappearance of the Er moment in the 4e sites observed in $Er_3Cu_4Sn_4$ below the Néel temperature, determined in this case by the magnetic ordering in the 2d sites, is also observed in the isostructural $R_3Cu_4Ge_4$ [10] and $RTGe_2$ [3–5] compounds and is connected with a weaker coupling between the magnetic moments within this sublattice and between the 2d and 4e sublattices.

The volume effects observed in the studied compounds may also affect their magnetic behaviour.

Acknowledgments

This work was partially supported by the European Commission under the Access to Research Infrastructures of the Human Potential Programme (contract number HPRI-CT-1999-00020) and IHP II Programme (project number: 466) and by the State Committee for Scientific Research in Poland within the confines of the Grant 2P03B 113 23. The authors (EW, BP and AS) would like to express their gratitude to the management of the Berlin Neutron Scattering Centre for the financial support and kind hospitality. WS thanks the State Committee for Scientific Research in Poland.

References

[1] Sholozdra R V, Komarovskaya L P and Akselnid L G 1984 *Ukr. Fiz. Zh.* **29** 1395
[2] Français M, Venturini G, McRae E, Malaman B and Rogues B 1987 *J. Less-Common Met.* **128** 249
[3] Schmitt D, Ouladdiaf D, Routsi Ch D, Yakinthos J K and Gamari-Seale H 1999 *J. Alloys Compounds* **292** 21
[4] Penc B, Hofmann M, Szytuła A and Zygmunt A 2001 *J. Phys.: Condens. Matter* **13** 4471
[5] Gil A, Penc B, Hofmann M, Szytuła A and Zygmunt A 2001 *J. Alloys Compounds* **322** 21
[6] Singh S, Dhar S K, Manfrinetti P and Palenzona A 2000 *J. Alloys Compounds* **298** 68
[7] Zaharko O, Keller L and Ritter C 2002 *J. Magn. Magn. Mater.* **253** 130
[8] Singh S, Dhar S K, Manfrinetti P and Palenzona A 2002 *J. Magn. Magn. Mater.* **250** 190
[9] Zaharko O and Keller L 2001 *Scientific Report* (Villigen: Paul Scherrer Institute) p 24

[10] Wawrzyńska E, Hernandez-Velasco J, Penc B, Szytuła A and Zygmunt A 2003 Magnetic structures of $R_3Cu_4Ge_4$ (R = Tb, Dy, Ho and Er) *J. Magn. Magn. Mater.* at press
[11] Rodriguez-Carvajal J 1993 *Physica* B **192** 55
[12] Bertaut E F 1968 *Acta Crystallogr.* A **24** 217
[13] Izyumov Y A 1990 *Phase Transitions and Crystal Symmetry* (Dordrecht: Kluwer–Academic)
[14] Sikora W 1994 *Proc. Symmetry and Structural Properties of Condensed Matter (Zajączkowo, Poland)* p 484
[15] Kovalev O V 1993 *Representations of the Crystallographic Space Groups* ed H T Stokes and D M Hatch (Switzerland: Gordon and Breach)
[16] de Gennes P G 1962 *J. Phys. Rad.* **23** 510
de Gennes P G 1962 *J. Phys. Rad.* **23** 630
[17] Noakes D R and Shenoy G H 1982 *Phys. Lett.* A **91** 35
[18] Gignoux D and Schmitt D 1993 *Phys. Rev.* B **48** 142682